



The detection of polyamines by an extended gate-type organic transistor functionalized with a carboxylate attached 1,3,4-thiadiazole derivative

Journal:	<i>Journal of Materials Chemistry C</i>
Manuscript ID	TC-ART-04-2021-001542.R1
Article Type:	Paper
Date Submitted by the Author:	06-May-2021
Complete List of Authors:	Asano, Koichiro; The University of Tokyo, Institute of Industrial Science Sasaki, Yui; The University of Tokyo, Institute of Industrial Science Zhou, Qi; The University of Tokyo Institute of Industrial Science, Mitobe, Riho; The University of Tokyo, Institute of Industrial Science Tang, Wei; The University of Tokyo, Institute of Industrial Science Lyu, Xiaojun; The University of Tokyo Institute of Industrial Science, Kamiko, Masao; The University of Tokyo, Institute of Industrial Science Tanaka, Hikaru; Toyobo Co.,Ltd., Corporate Research Center Yamagami, Akari; Toyobo Co.,Ltd., Corporate Research Center Hagiya, Kazutake; Toyobo Co.,Ltd., Corporate Research Center Minami, Tsuyoshi; The University of Tokyo, Institute of Industrial Science

ARTICLE

The detection of polyamines by an extended gate-type organic transistor functionalized with a carboxylate attached 1,3,4-thiadiazole derivative

Received 00th January 20xx,
Accepted 00th January 20xx

DOI: 10.1039/x0xx00000x

Koichiro Asano,^a Yui Sasaki,^a Qi Zhou,^a Riho Mitobe,^a Wei Tang,^a Xiaojun Lyu,^a Masao Kamiko,^a Hikaru Tanaka,^b Akari Yamagami,^b Kazutake Hagiya,^b and Tsuyoshi Minami^{a*}

We herein report an extended gate-type organic thin-film transistor (OTFT)-based polyamine sensor and its application for pattern recognition. The extended-gate electrode was functionalized with a complex of copper(II) ions and 2-carboxymethylthio-5-mercapto-1,3,4-thiadiazole, which enabled the OTFT to respond to polyamines in an aqueous solution. Moreover, the responses of the OTFT-based sensor exhibited a cross-reactivity, implying its capability of detecting multi-analytes. Thus, we performed pattern recognition against nine target polyamines (spermine, spermidine, trimethylenediamine, ethylenediamine, histamine, tryptamine, putrescine, cadaverine and 1,6-diaminohexane) in combination with linear discriminant analysis and successfully discriminated the analytes. Moreover, we achieved the quantification of spermine in a diluted fruit juice by a support vector machine with high accuracy. Overall, the demonstration using the OTFT-based chemical sensor with pattern recognition revealed a potential for sensing polyamines in real samples.

1. Introduction

Naturally existing in food, polyamines such as spermine are reported to be essential components of living cells and are known as representative biomarkers for cancer and age-associated diseases.¹⁻⁴ Thus, the qualitative and quantitative analysis of polyamines has been highly demanded in food analysis and diagnosis.⁵⁻⁹ Conventional instrumental methods (including high-performance liquid chromatography (HPLC)¹⁰⁻¹² and gas chromatography-mass spectrometry (GC-MS)¹³⁻¹⁵, etc.) for detecting polyamines can achieve highly accurate analysis, whereas these methods require large equipment, technically trained personnel, and complicated pretreatment processes for the samples. Besides, although facile analytical methods such as optical sensors with spectrophotometers have been developed for the easy-to-recognize amines,¹⁶⁻²¹ miniaturized sensing platforms are still desirable for achieving onsite polyamine sensing. In this regard, organic thin-film transistors (OTFTs) have raised broad attention. The OTFTs are light-weight flexible semiconductor devices, which can be fabricated on plastic films²²⁻²⁴ and serve as promising sensor platforms upon the functionalization of molecular recognition materials.²⁵⁻²⁸ Among them, an extended gate-type OTFT can give a quantitative and stable response upon the change in analyte concentration that would cause the surface potential change on the extended-gate electrode.²⁹⁻³³ In

a previous report, an OTFT has succeeded in the detection of diamines by a diamine oxidase functionalized on the gold (Au) extended-gate electrode, while the capability of discrimination of polyamine species is still concerned.³⁴⁻³⁶ On the other hand, artificial

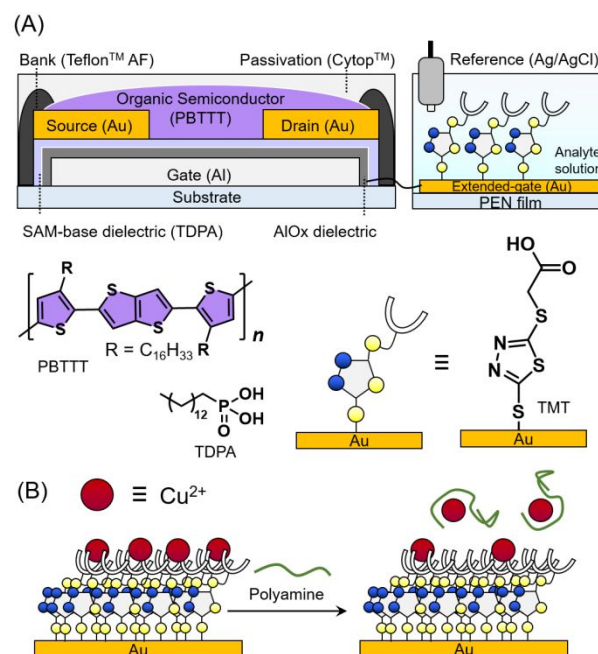


Fig. 1 (A) Schematic illustration of the organic transistor-based polyamine sensor and chemical structures of components for the device. (B) Conceptual illustration of the polyamine detection mechanism.

^a Institute of Industrial Science, The University of Tokyo, 4-6-1 Komaba, Meguro-ku, Tokyo, 153-8505, Japan. E-mail: tminami@iis.u-tokyo.ac.jp

^b Corporate Research Center, Toyobo Co., Ltd., 2-1-1 Katata, Otsu, Shiga, 520-0292, Japan.

Electronic Supplementary Information (ESI) available: Characterization and fabrication details of the extended-gate OTFT, EIS, titrations, XPS, reusability test, LDA and SVM. See DOI: 10.1039/x0xx00000x

receptors show a cross-reactivity,²⁵ implying that the artificial receptor-based chemical sensors could recognize multi-analytes with pattern recognition techniques.³⁷⁻⁴¹

1,3,4-Thiadiazole and its derivatives possess highly polarizable structures and rich electron density, these properties of which offer the capability of demonstrating distinct electrochemical potential changes.^{42, 43} However, despite being widely researched in organic electronics (*e.g.*, organic solar cells^{42, 44, 45} and organic light-emitting diodes^{46, 47}), the application of 1,3,4-thiadiazole and its derivatives on electrodes has not been widely reported. This is probably due to the instability of self-assembled monolayers (SAMs) of thiadiazole derivatives. An X-ray photoelectron spectroscopy (XPS) evidence revealed that such a SAM consisted of 2-mercapto-5-methyl-1,3,4-thiadiazole on Au decomposed at room temperature.⁴⁸ However, another previous literature reported that the above thiadiazole derivative could form a stable SAM layer.⁴⁹ Thus, we have been interested in investigating thiadiazole derivatives on the Au surface and their applications. With the consideration of the electron density and conductive ability of thiadiazole derivatives functionalized on the Au surface, 2-carboxymethylthio-5-mercapto-1,3,4-thiadiazole (TMT) was selected. According to the chemical structure of TMT, its SAM was expected to perform as a two-dimensional molecular recognition scaffold, which could lead to quantitative detection in combination with sensing transducers (*i.e.*, OTFTs). Besides, since polyamines exhibit different binding affinities to the copper(II) ion (Cu^{2+}), a competitive assay among TMT, Cu^{2+} and polyamines on the extended-gate electrode was employed. Notably, the competitive manner could contribute to achieving multi-responses for pattern recognition.^{40, 50} In other words, even a single OTFT-based sensor has the potential to discriminate various polyamines simultaneously based on the above competitive assay. Therefore, we demonstrated the detection and discrimination of multi-polyamines based on the combination of the Cu^{2+} -TMT functionalized OTFT and pattern recognition (*i.e.*, linear discriminant analysis (LDA)^{38, 39} and support vector machine (SVM)^{51, 52}). Considering the importance of polyamines such as spermine in food analysis, we further attempted to use the functionalized OTFT device to detect spermine levels in a fruit juice.⁵³

2. Experimental

2.1 Reagents and materials

Reagents and solvents were purchased from commercial suppliers and used without further purification. TMT and polyethylene naphthalate (PEN) film were supplied by Toyobo Co., Ltd. Copper(II) perchlorate hexahydrate, spermine tetrahydrochloride, spermidine, 5-carboxy-1-pentanethiol, and histamine dihydrochloride were purchased from Sigma-Aldrich Co. LLC. Ethylenediamine anhydrous, 1,3-diaminopropane (trimethylenediamine), 1,4-diaminobutane (putrescine), 1,5-diaminopentane (cadaverine) dihydrochloride, 1,6-diaminohexane dihydrochloride, methylamine hydrochloride, tryptamine hydrochloride and 4-mercaptobenzoic acid were purchased from Tokyo Chemical Industry Co. Ltd. Sodium chloride was purchased from Kanto Chemical Co. Inc. *N*-Cyclohexyl-2-aminoethanesulfonic acid (CHES) and 4-(2-hydroxyethyl)-1-piperazineethanesulfonic acid (HEPES) were purchased from Dojindo Laboratories. Poly{2,5-bis(3-hexadecylthiophene-2-yl)thieno[3,2-

b]thiophene (PBTtT) was purchased from Merck KGaA. An amorphous fluoropolymer Cytop™ (model: CTX-809M) and perfluorotributylamine were supplied by AGC Co. Ltd. Glass substrates (model: Eagle XG, 2 cm × 2.5 cm) was purchased from Corning, Inc. Aluminum (Al) wire (1φ) and Gold particle (Au) for vacuum deposition were purchased from Furuuchi Chemical Co., Ltd. and Tanaka Kikinzoku Kogyo Co., Ltd., respectively. Aqueous solutions for all experiments were prepared using Mill-Q water (18.2 MΩ cm).

2.2 Measurements

Photoelectron yield spectroscopy (PYS) measurements in air were performed using an AC-3 from Riken Keiki, Co. Wettability measurements were performed by a CA-X contact angle meter from Kyowa Interface Science, Co. Ltd. XPS was measured by an ULVAC PH-Quantera spectrometer. The pH values of solutions were measured using a Seven Excellence pH meter from Mettler-Toledo, Ltd. The infrared (IR) spectra were measured using a Fourier transform infrared spectrophotometer (FT-IR) (model: Nicolet iS5 from Thermo Fisher Scientific Inc), equipped with a variable angle grazing angle ATR from Harrick Scientific Products. The linear sweep voltammetry (LSV), cyclic voltammetry (CV) and electrochemical impedance spectroscopy (EIS) were operated on an SP-300 potentiostat from Biologic. The Ag/AgCl reference electrode (RE-1B) and Pt wire counter electrode were purchased from BAS, Inc. Electrical characteristics of all OTFT devices were measured using Keithley 2602B and 2612B source meters.

2.3 Fabrication of the OTFT-based chemical sensor

The extended gate-type OTFT sensor is designed to isolate the operation part (*i.e.*, OTFT) from the detection part (*i.e.*, extended-gate electrode) for stable detection in aqueous media.³⁰ The main OTFT part, which could be operated at low drive voltage ($<|3|$ V), was accomplished by functionalizing aluminium oxide (AlO_x) with the usage of tetradecylphosphonic acid (TDPA) as the gate dielectric layer.⁵⁴ The fabrication process was completed using solution-processable PBTtT as the active layer,⁵⁵ protected with a fluoropolymer (CYTOP™) afterwards. More details of the reagents, instruments, and the fabrication process involved for the OTFT device are summarized in the Electronic Supplementary Information (ESI).

2.4 Fabrication and characterization of the extended-gate electrode

The extended-gate electrode, which contains a gold-made detection part (100 nm thickness with 15 mm² sensing area), was prepared through the thermal evaporation of gold on a polyethylene naphthalate (PEN) film (125 μm thickness). The electrode was then washed using Milli-Q water and methanol, followed by drying with nitrogen gas flow. Next, the electrode was washed using a UV-O₃ cleaner (ASUMI-GIKEN, ASM401 OZ) for 10 min before the following modification. After this period, the extended-gate electrode was immersed in a methanol solution of 10 mM TMT for 1 h at 25 °C. The electrode was then washed and dried using methanol and immersed into a HEPES buffer solution (100 mM, pH 7.4 at 25 °C) containing 1 mM $\text{Cu}(\text{ClO}_4)_2$. Before all the electrochemical characterization experiments, the background solution was bubbled with N₂ flow for

20 min for eliminating dissolved oxygen. The density of the TMT molecule on the extended-gate electrode was estimated by the LSV method in a KOH solution (0.1 M), with potential scanning from 0 V to -1.6 V (vs. Ag/AgCl) at 20 mV/s. Besides, the modified electrodes were further characterized by CV and EIS with a three-electrodes system in a Na_2SO_4 background solution (0.1 M). The modified electrode, the Ag/AgCl electrode (with NaCl salt bridge), and a Pt wire electrode were used as the working electrode, reference electrode and counter electrode, respectively. For CV experiments, the potential range was set to $-0.6 - 0.6$ V (vs. Ag/AgCl) with a scanning rate of 20 mV/s. For EIS experiments, the applied potential was set at the open circuit potential of the working electrode, and the frequency range was set as 5 MHz to 0.1 Hz with an amplitude potential of 5 mV.

3. Results and discussion

3.1 Characterization of the extended-gate electrode

The TMT-based SAM on the extended-gate electrode was characterized by PYS in air, the contact angle measurement, XPS, FT-IR (ATR), and LSV. The work function of the TMT treated Au electrode was deeper than that of the untreated Au (Fig. 2(A)), which was probably due to an electron-withdrawing group (*i.e.*, the carboxy group).⁵⁶ Furthermore, the decrease in the contact angle in Fig. 2(B) suggested the immobilization of the hydrophilic monolayer on the extended-gate electrode. The results of XPS revealed peaks of all elements of the TMT-based SAM (*e.g.*, N1s, O1s, S2p). In the previous report, the peak originated from S2p was observed at *ca.* 164-165 eV in 2-mercapto-5-methyl-1,3,4-thiadiazole.⁴⁹ In our case, a similar peak derived from S2p of TMT was also observed at *ca.* 164-165 eV, reflecting the similarity in the structure of the thiolated thiadiazole derivative and TMT. Besides, the peaks of O1s and N1s indicated that TMT formed the stable SAM without decomposition. In addition, we observed absorption peaks originating from C=O stretching vibration (1711 cm^{-1}) and C-H stretching vibration (2852 cm^{-1} and 2922 cm^{-1}). Moreover, a broad peak stemming from O-H stretching vibration exhibited at a range from 3000 cm^{-1} to 3300 cm^{-1}

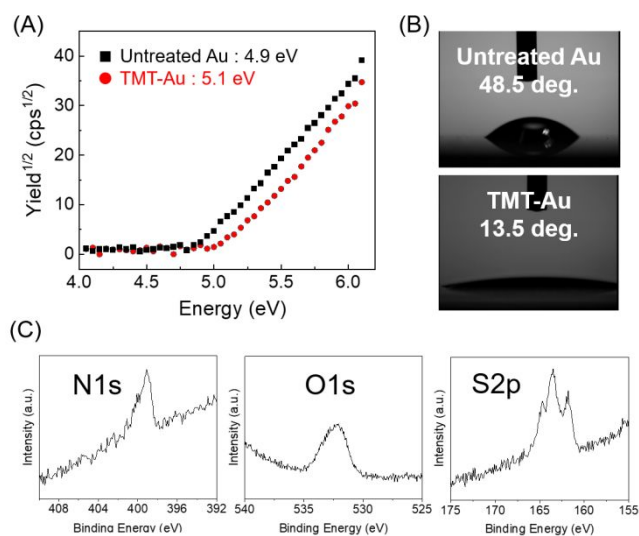


Fig. 2 Characterization of the TMT SAM on the extended-gate electrode by (A) PYS, (B) contact angle measurement, and (C) XPS.

(See the ESI). Besides, the density of TMT on the extended-gate electrode was estimated to 9.7×10^{-10} mol/cm² by the LSV method⁵⁷ (See the ESI). Overall, the extended-gate electrode was successfully functionalized by the TMT-based SAM.

3.2 Evaluation of Cu^{2+} binding to the TMT SAM on the electrode

We utilized CV and EIS to characterize the electrodes after the functionalization. The CV results of the electrodes are shown in Fig. 3(A). The black dot line, red dash line and blue solid line indicate the untreated Au electrode, the TMT-modified electrode, and the Cu^{2+} -TMT modified electrode, respectively. In the case of the TMT-modified electrode, there was an obvious reduction peak at *ca.* -0.4 V, indicating the reduction of the thiol group from the Au extended-gate electrode. On the other hand, no peak appeared at *ca.* -0.4 V in

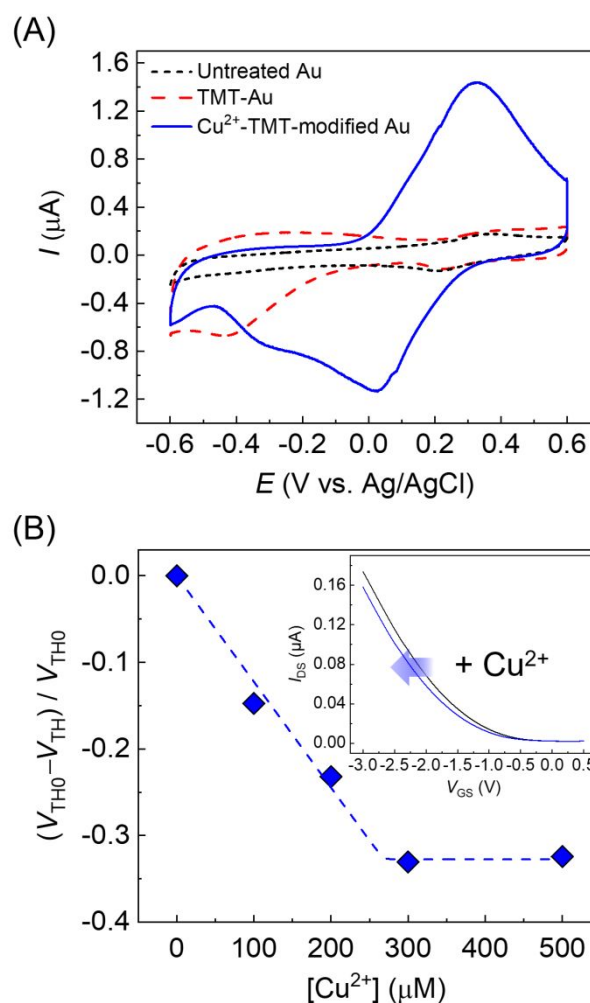


Fig. 3 (A) Cyclic voltammetry of the untreated Au electrode (black dot line), TMT-Au electrode (red dash line), and Cu^{2+} -TMT-Au electrode (blue solid line) in the Na_2SO_4 solution (0.1 M). Potential range: $-0.6 - 0.6$ V (vs. Ag/AgCl), scan rate: 20 mV/s. The Cu^{2+} -TMT complex was clearly observed with the typical reduction and oxidation peaks of copper ions. (B) Changes in the threshold voltage of the OTFT functionalized with the TMT SAM upon the addition of Cu^{2+} in a 100 mM HEPES buffer solution at pH 7.4 at 25 °C. Inset shows the shift of the transfer characteristics ($V_{\text{DS}} = -1$ V) of the OTFT by adding Cu^{2+} (500 μM).

the case of the untreated extended-gate electrode. After the TMT-modified electrode incubated with Cu^{2+} ions, a new reduction peak (at *ca.* 0.0 V) and an oxidation peak (at *ca.* 0.3 V) were observed, which matched with the reduction and oxidation process of the copper ion. Besides, the charge-transfer resistance of these electrodes was also analyzed by comparing the diameter of the semicircle in Nyquist plots (Fig. S4). The untreated Au electrode exhibited the lowest resistance, while the resistance was increased after the TMT modification, due to the charge transfer process prevented by the TMT SAM. Nevertheless, the resistance decreased after the incubation with the Cu^{2+} ion, implying the increase of the ion concentration on the surface of the TMT-modified electrode. To support the complexation on the SAM, the Cu^{2+} -TMT SAM modified Au electrode was characterized by XPS and PYS. The XPS results revealed the appearance of the Cu2p peak. Besides, the shift of work function was observed in the PYS measurement (Fig. S2). Thus, the functionalization process was comprehensively studied with electrochemical methods, XPS, and PYS, and the decoration of the Cu^{2+} -TMT complex SAM on the electrode was successfully evaluated.

Next, we evaluated the effect of Cu^{2+} -TMT complex on the OTFT performance in aqueous media. The OTFT showed transistor characteristics with almost no hysteresis (Fig. S6), indicating that the OTFT can be used as a chemical sensor. As shown in Fig. 3(B), the OTFT functionalized with the TMT-based SAM exhibited a negative shift with increasing Cu^{2+} concentration in a buffer solution. The change in the threshold voltage (V_{th}) of the OTFT corresponded to the increase of the Cu^{2+} concentration, and the transistor response finally saturated. The observed OTFT response suggests that the changes in the surface potential were induced because the Cu^{2+} ion was captured on the surface of the SAM.²⁹ Therefore, we decided to apply the OTFT functionalized with the Cu^{2+} -TMT SAM electrode to polyamine sensing.

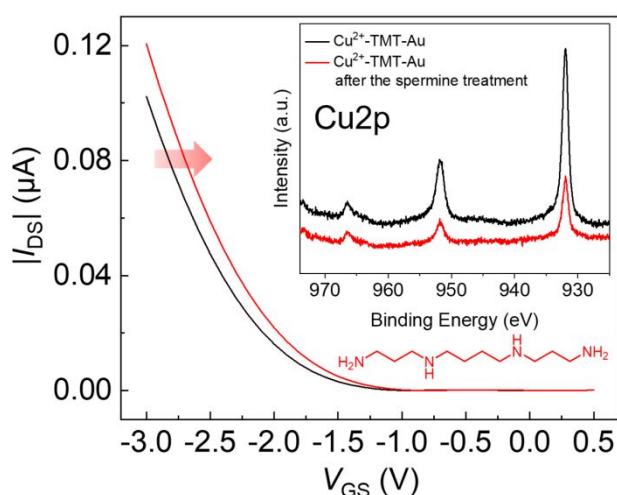


Fig. 4 Change in transfer characteristics ($V_{\text{GS}}^-I_{\text{DS}}$) of the OTFT-based sensor upon the addition of spermine (150 μM) in a 50 mM CHES buffer solution with 10 mM NaCl at pH 8.5 at 25 °C ($V_{\text{DS}} = -1$ V). Inset represents the changes in the intensity of the Cu2p peaks after the treatment of spermine, obtained by the XPS measurement.

3.3 Polyamine detection

In this assay, the electrical response of the OTFT-based sensor with the Cu^{2+} -TMT SAM electrode was evaluated against ten amines (*i.e.*, spermine, spermidine, 1,6-diaminohexane, trimethylenediamine, cadaverine, ethylenediamine, putrescine, methylamine, histamine, and tryptamine). Because the complex of Cu^{2+} and a polyamine (*e.g.*, spermine) can be formed at basic conditions ($> \text{pH } 8$),⁵⁸ the amine sensing was carried out in the CHES buffer solution (50 mM) with NaCl (10 mM) at pH 8.5. As shown in Fig. 4, the transistor characteristics changed upon the addition of spermine, and the titration isotherm was obtained by collecting V_{th} at various spermine concentrations. The Cu^{2+} -TMT SAM attached OTFT showed a positive shift toward spermine, in comparison to the negative shift toward the Cu^{2+} ion. The change is probably due to the removal of Cu^{2+} from the Cu^{2+} -TMT SAM induced by the complexation of the Cu^{2+} ion and spermine.⁵⁹ Indeed, the intensity of the Cu2p peak in XPS decreased after the treatment of the Cu^{2+} -TMT electrode with spermine (Fig. 4 inset), which supported the positive shift of the OTFT characteristics. The limit of detection was estimated to be 0.4 ppm based on the 3 σ method.⁶⁰

To clarify the role of the TMT-based SAM for efficient amine sensing, we also performed spermine detection using 4-mercapto benzoic acid and 5-carboxy-1-pentanethiol based SAMs in the presence of Cu^{2+} . Thus we could investigate how difference in the

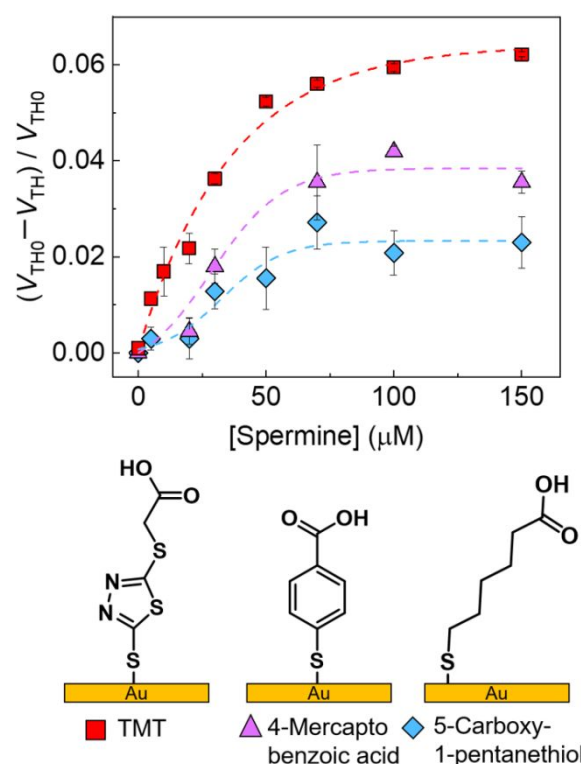


Fig. 5 Comparison of changes in the threshold voltage of the OTFTs upon the addition of spermine. [Spermine] = 0 – 150 μM . The OTFTs were functionalized with the SAMs of carboxylate derivatives with Cu^{2+} ions. TMT: red square, 4-mercapto benzoic acid: purple triangle, and 5-carboxy-1-pentanethiol: blue diamond. Each electrode was evaluated in a 50 mM CHES buffer solution with 10 mM NaCl at pH 8.5 at 25 °C.

SAM structures affect the detection sensitivity (Fig. 5). The TMT-based OTFT sensor showed the most distinguished potential changes for detecting spermine. This property derives from the unique structure of TMT. Comparing with 5-carboxy-1-pentanethiol, the thiadiazole unit in TMT could offer a conductive path for the fast transfer of electrons to the surface of the electrode. Besides, the nitrogen and sulfur atoms in the structure of TMT greatly increased the electron density in the whole structure,⁶¹ in comparison to the 4-mercapto benzoic acid. To support this hypothesis, we also tested the charge-transfer resistance of TMT and 4-mercapto benzoic acid-modified Au electrodes by EIS. The TMT modified Au electrode showed lower resistance, demonstrating that electrons could more easily transfer through the TMT SAM. Moreover, the molecular density of the three receptors on the Au surface could also contribute to the response difference (See ESI). Thus, with the conductive property, the rich electron density in the structure and the molecular density, TMT-based SAM revealed excellent performance in spermine detection.

3.4 Selectivity test and Pattern recognition of polyamines

As a further investigation, the selectivity test against ten amines was operated. In Fig. 6, the OTFT-based sensor exhibited different

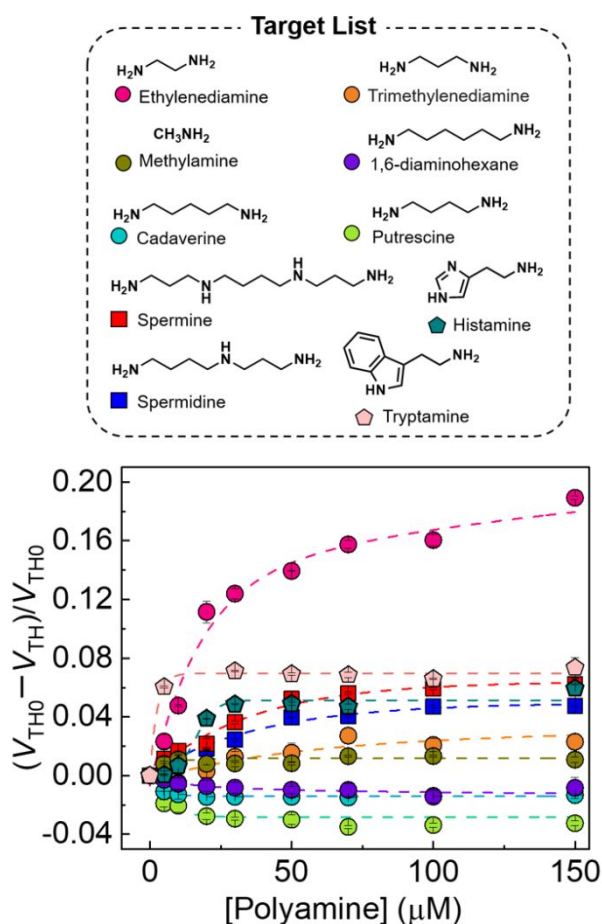


Fig. 6 Chemical structures of the target polyamines and the result of selectivity test against ten polyamines. The sensing abilities were evaluated in a 50 mM CHES buffer solution with 10 mM NaCl at pH 8.5 at 25 °C. [Polyamine] = 0 – 150 μM.

response patterns corresponding to various amine structures. Remarkably, the response patterns obtained contain both positive and negative shifts of the OTFT characteristics. The cross-reactive response pattern attributes to the difference in binding modes and affinities among Cu^{2+} ions, TMT and the target amines. The positive V_{th} shifts could be derived from the removal of Cu^{2+} upon the addition of polyamines, such as ethylenediamine, spermine, spermidine, and trimethylenediamine, histamine, and tryptamine. While the negative shifts were probably due to the accumulation of target amines such as 1,6-diaminohexane, cadaverine, and putrescine on the Cu^{2+} -TMT SAM. To explore the key leading to these phenomena, we characterized these electrodes by XPS. The intensity of the Cu2p peak decreased after the Cu^{2+} -TMT SAM that was incubated with amines, while the decreasing extent was different. For example, the decrease of the Cu2p peak intensity by adding spermine was more significant than by adding putrescine (Fig. S11(A)). Besides, We also observed the formation of a new broad peak in XPS of N1s after the Cu^{2+} -TMT SAM that was incubated with putrescine (Fig. S11(B)), meaning the adsorption of putrescine on the SAM. Thus, the difference in the surface conditions of electrodes could lead to positive or negative responses to polyamines. The highest response to ethylenediamine was derived from its extremely high binding affinity for Cu^{2+} ions ($\log K_{11} = 11$ and $\log K_{12} = 21$ in water).⁶² On the other hand, methylamine induced almost no response of the OTFT due to its monoamine structure. Given the fact in the cross-reactivity, it could be stated that the OTFT has a potential for multi-polyamine detection.

To demonstrate pattern recognition of polyamines using the OTFT-sensor, we employed LDA. LDA is one of the supervised methods to discriminate components based on the similarities among the analytes with decreasing dimensions of inset data.^{38, 39} In this assay, the dataset composes the relative changes of drain current (I_{DS}) in transfer characteristics obtained by amine addition at $V_{\text{GS}} = 0.5 - -3$ V. Fig. 7 represented the LDA canonical score plots, and nine analytes were discriminated with a 100% correct classification rate. The position of each cluster corresponded to the direction of V_{th} shifts derived from the polyamine detection. Among them, the distance of clusters of histamine and tryptamine were close, indicating that the OTFT-based chemical sensor succeeded not only in the multi-amine discrimination but also in grouping amines based on the similarity of the chemical information.

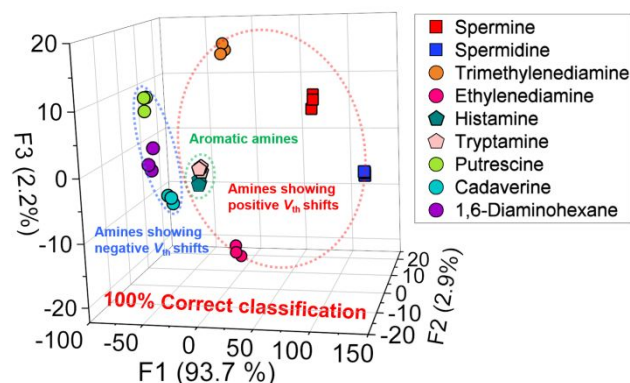


Fig. 7 LDA canonical score plots for nine polyamines with a 100% correct classification. [Polyamine] = 150 μM.

Finally, we examined the potential utility of the proposed device using a commercial mango juice.⁵³ Aforementioned, spermine is one of the important biomarkers and widely exists in food. To establish a rapid and easy-to-operate method to quantify the amount of spermine, we carried out the quantitative analysis with SVM. The SVM analysis contains two datasets: the calibration dataset to build the model and the prediction dataset for predicting the unknown target concentrations.^{51,52} Different concentrations of spermine were mixed with the diluted mango juice, and the spermine concentration in the solution was predicted based on the calibration model by the titration of the standard spermine solutions. It is worth mentioning that the analysis of multi-concentrations was achieved in the mixture solutions with high accuracy (Fig. S13). Thus, the result indicated that the proposed OTFT-based chemical sensor would be applied to the quantification of spermine in the practical range (< 150 μ M) in the food samples.

Conclusions

We demonstrated polyamine detection using an OTFT-based chemical sensor in an aqueous media. The sensing portion was a Cu^{2+} -TMT SAM functionalized extended-gate electrode. We successfully characterized the Cu^{2+} -TMT SAM on the Au extended-gate electrode by several analytical methods including the contact angle measurement, PYS, XPS, FT-IR (ATR), and electrochemical measurements. As a result, we found that the TMT SAM was stable on the Au surface. Besides, based on the removal of Cu^{2+} ions from the Cu^{2+} -TMT SAM upon the addition of polyamines, the fabricated OTFT exhibited a response with an increasing polyamine concentration. In addition, the rich electron density, the conductive property, and the molecular density that originated from the structure of TMT enabled the higher response to spermine compared with 4-mercapto benzoic acid and 5-carboxy-1-pentanethiol. Furthermore, the selectivity test to ten amines was operated by the Cu^{2+} -TMT SAM attached OTFT, and different response pattern (*e.g.*, positive and negative responses) to different polyamines was observed. This phenomenon was derived from the different amounts of Cu^{2+} ions and polyamines on the SAM after the incubation with polyamines, which was confirmed by the XPS measurements.

We performed pattern recognition for nine polyamines using the Cu^{2+} -TMT SAM attached OTFT in combination with LDA. The OTFT successfully discriminated nine polyamines with 100% correct classification, and its grouping was achieved based on the similarity of the chemical information. In other words, the demonstration revealed the potential of the Cu^{2+} -TMT SAM attached OTFT sensor for multi-analyte detection. In addition, the OTFT was applied to detect spermine in a commercial fruit juice to evaluate a capability for food analysis with SVM.

Overall, we demonstrated multi-polyamine detection by the OTFT for the first time. Our approach based on the competitive assay would be able to broaden the avenue for easy-to-analyze onsite detection methods for multi-targets.

Author Contributions

KA operated FT-IR, contact angle, PYS and tested the OTFT performance. YS performed pattern recognition and wrote the manuscript. QZ performed the electrochemical experiments and wrote the manuscript. RM fabricated the OTFT, carried out OTFT titrations, and measured XPS with MK. WT contributed to writing the manuscript and performed SVM with XL. HT, AY, and KH supplied TMT. TM conceived the entire project.

Conflicts of interest

There are no conflicts of interest to declare.

Acknowledgements

TM thanks the Japan Society for the Promotion of Science (JSPS KAKENHI Grant Numbers JP20K21204 and JP20H05207), and JST CREST (Grant No. JPMJCR2011). YS also thanks JSPS, Research Fellow for Young Scientists (PD), No. JP18J21190. We appreciate professor Shunsuke Yagi and Mengqiao Wang for their helpful discussion.

References

1. R. A. Casero, T. Murray Stewart and A. E. Pegg, *Nat. Rev. Cancer*, 2018, **18**, 681-695.
2. S. Bardócz, T. J. Duguid, D. S. Brown, G. Grant, A. Pusztai, A. White and A. Ralph, *Br. J. Nutr.*, 1995, **73**, 819-828.
3. M. K. Andersen, T. S. Høiem, B. S. R. Claes, B. Balluff, M. Martin-Lorenzo, E. Richardsen, S. Krossa, H. Bertilsson, R. M. A. Heeren, M. B. Rye, G. F. Giskeødegård, T. F. Bathen and M.-B. Tessem, *Cancer Metab.*, 2021, **9**, 9.
4. L. A. Vandergrift, E. A. Decelle, J. Kurth, S. L. Wu, T. L. Fuss, E. M. DeFeo, E. F. Halpern, M. Taupitz, W. S. McDougal, A. F. Olumi, C. L. Wu and L. L. Cheng, *Sci. Rep.*, 2018, **8**, 12.
5. X. Gong, N. L. Qi, X. X. Wang, L. J. Lin and J. H. Li, *Food Chem.*, 2014, **162**, 172-175.
6. B. Karayigit, N. Colak, F. Ozogul, A. Gundogdu, H. Inceer, N. Bilgili and F. A. Ayaz, *Food Biosci.*, 2020, **37**, 14.
7. M. N. Roselino, L. F. Maciel, V. Sirocchi, M. Caviglia, G. Sagratini, S. Vittori, M. P. Taranto and D. C. U. Cavallini, *J. Food Compos. Anal.*, 2020, **94**, 7.
8. P. K. F. Chiu, Y. H. Fung, J. Y. C. Teoh, C. H. Chan, K. L. Lo, K. M. Li, R. T. H. Tse, C. H. Leung, Y. P. Wong, M. J. Roobol, K. L. Wong and C. F. Ng, *Prostate Cancer Prostatic Dis.*, DOI: 10.1038/s41391-020-00312-1, 7.
9. S. Saiki, Y. Sasazawa, M. Fujimaki, K. Kamagata, N. Kaga, H. Taka, Y. Z. Li, S. Souma, T. Hatano, Y. Imamichi, N. Furuya, A. Mori, Y. Oji, S. I. Ueno, S. Nojiri, Y. Miura, T. Ueno, M. Funayama, S. Aoki and N. Hattori, *Ann. Neurol.*, 2019, **86**, 251-263.
10. D. Yuan, J. J. Liu, H. Z. Zhang, N. Wang, H. Y. Zou, C. Z. Huang and J. Wang, *Talanta*, 2018, **188**, 218-224.
11. H. Jiang, X. Y. Rao, L. Li and Z. D. Liu, *Analyst*, 2020, **145**, 7673-7679.
12. D. Cao, X. Xu, X. Feng and L. Zhang, *Food Chem.*, 2020, **333**, 127518.

13. J. Pradenas, O. Galarce-Bustos, K. Henriquez-Aedo, R. Mundaca-Urbe and M. Aranda, *Food Control*, 2016, **70**, 138-144.
14. J. O. Fernandes and M. A. Ferreira, *J. Chromatogr. A*, 2000, **886**, 183-195.
15. L. Molognoni, H. Daguer, L. A. D. Ploencio and J. D. Lindner, *Talanta*, 2018, **178**, 1053-1066.
16. N. Kaur, S. Chopra, G. Singh, P. Raj, A. Bhasin, S. K. Sahoo, A. Kuwar and N. Singh, *J. Mater. Chem. B*, 2018, **6**, 4872-4902.
17. T. Minami, N. A. Esipenko, B. Zhang, L. Isaacs and P. Anzenbacher, *Chem. Commun.*, 2014, **50**, 61-63.
18. T. L. Nelson, C. O'Sullivan, N. T. Greene, M. S. Maynor and J. J. Lavigne, *J. Am. Chem. Soc.*, 2006, **128**, 5640-5641.
19. R. R. Nair, S. Debnath, S. Das, P. Wakchaure, B. Ganguly and P. B. Chatterjee, *ACS Appl. Bio Mater.*, 2019, **2**, 2374-2387.
20. K. Kumar, S. Kaur, S. Kaur, G. Bhargava, S. Kumar and P. Singh, *J. Mater. Chem. B*, 2019, **7**, 7218-7227.
21. J. R. Huang, W. J. Ye, S. Zha, Y. Z. Tao, M. Yang, K. Huang, J. Q. Liu, Y. H. Fung, Y. Li, P. H. Li, L. Z. Zhu and C. S. Lee, *J. Lumin.*, 2021, **232**, 9.
22. M. Y. Lee, H. R. Lee, C. H. Park, S. G. Han and J. H. Oh, *Acc. Chem. Res.*, 2018, **51**, 2829-2838.
23. L. Kergoat, B. Piro, M. Berggren, G. Horowitz and M.-C. Pham, *Anal. Bioanal. Chem.*, 2012, **402**, 1813-1826.
24. L. Torsi, M. Magliulo, K. Manoli and G. Palazzo, *Chem. Soc. Rev.*, 2013, **42**, 8612-8628.
25. R. Kubota, Y. Sasaki, T. Minamiki and T. Minami, *ACS Sens.*, 2019, **4**, 2571-2587.
26. H. Li, W. Shi, J. Song, H.-J. Jang, J. Dailey, J. Yu and H. E. Katz, *Chem. Rev.*, 2019, **119**, 3-35.
27. Y. Jang, M. Jang, H. Kim, S. J. Lee, E. Jin, J. Y. Koo, I.-C. Hwang, Y. Kim, Y. H. Ko, I. Hwang, J. H. Oh and K. Kim, *Chem*, 2017, **3**, 641-651.
28. T. Minamiki, T. Minami, Y.-P. Chen, T. Mano, Y. Takeda, K. Fukuda and S. Tokito, *Commun. Mater.*, 2021, **2**, 8.
29. P. Bergveld, *Sens. Actuators B Chem.*, 2003, **88**, 1-20.
30. T. Minamiki, T. Minami, R. Kurita, O. Niwa, S.-i. Wakida, K. Fukuda, D. Kumaki and S. Tokito, *Appl. Phys. Lett.*, 2014, **104**, 243703.
31. T. Minamiki, T. Minami, P. Koutnik, P. Anzenbacher and S. Tokito, *Anal. Chem.*, 2016, **88**, 1092-1095.
32. T. Kajisa and T. Sakata, *ACS Appl. Mater. Interfaces*, 2018, **10**, 34983-34990.
33. Q. Zhou, M. Wang, S. Yagi and T. Minami, *Nanoscale*, 2021, **13**, 100-107.
34. T. Minami, T. Sato, T. Minamiki and S. Tokito, *Anal. Sci.*, 2015, **31**, 721-724.
35. C. Li, Y. Wang, T. Zhang, B. Zheng, J. Xu and Q. Miao, *Chem. Asian J.*, 2019, **14**, 1676-1680.
36. J. Zhu, X. Wang and H. Wang, *Appl. Phys. A*, 2020, **126**, 463.
37. Y. Sasaki, R. Kubota and T. Minami, *Coord. Chem. Rev.*, 2021, **429**, 213607.
38. Z. Li, J. R. Askim and K. S. Suslick, *Chem. Rev.*, 2019, **119**, 231-292.
39. J. P. Anzenbacher, P. Lubal, P. Buček, M. A. Palacios and M. E. Kozelkova, *Chem. Soc. Rev.*, 2010, **39**, 3954-3979.
40. M. Kitamura, S. H. Shabbir and E. V. Anslyn, *J. Org. Chem.*, 2009, **74**, 4479-4489.
41. Y. Sasaki, S. Kojima, V. Hamedpour, R. Kubota, S. Takizawa, I. Yoshikawa, H. Houjou, Y. Kubo and T. Minami, *Chem. Sci.*, 2020, **11**, 3790-3796.
42. Y. Wang and T. Michinobu, *J. Mater. Chem. C*, 2016, **4**, 6200-6214.
43. S. Oprea, V. O. Potolinca and V. Oprea, *Eur. Polym. J.*, 2021, **143**, 9.
44. S. Fukuta, Z. Wang, S. Miyane, T. Koganezawa, T. Sano, J. Kido, H. Mori, M. Ueda and T. Higashihara, *Polym. J.*, 2015, **47**, 513-521.
45. Q. Fan, Y. Liu, M. Xiao, W. Su, H. Gao, J. Chen, H. Tan, Y. Wang, R. Yang and W. Zhu, *J. Mater. Chem. C*, 2015, **3**, 6240-6248.
46. A. K. Yadav, B. Pradhan, H. Ulla, S. Nath, J. De, S. K. Pal, M. Satyanarayan and A. S. Achalkumar, *J. Mater. Chem. C*, 2017, **5**, 9345-9358.
47. J. Jin, W. Zhang, B. Wang, G. Mu, P. Xu, L. Wang, H. Huang, J. Chen and D. Ma, *Chem. Mater.*, 2014, **26**, 2388-2395.
48. F. Hipler, S. Gil Girol, W. Azzam, R. A. Fischer and C. Wöll, *Langmuir*, 2003, **19**, 6072-6080.
49. J. Zhou, S. Chen, L. Zhang, Y. Feng and H. Zhai, *J. Electroanal. Chem.*, 2008, **612**, 257-268.
50. B. T. Nguyen and E. V. Anslyn, *Coord. Chem. Rev.*, 2006, **250**, 3118-3127.
51. L. H. Hamel, *Knowledge Discovery with Support Vector Machines*, Wiley, Hoboken, NJ, 2009.
52. T. Minami, N. A. Esipenko, B. Zhang, M. E. Kozelkova, L. Isaacs, R. Nishiyabu, Y. Kubo and P. Anzenbacher, *J. Am. Chem. Soc.*, 2012, **134**, 20021-20024.
53. M. Atiya Ali, E. Poortvliet, R. Strömberg and A. Yngve, *Food Nutr. Res.*, 2011, **55**, 5572.
54. H. Klauk, U. Zschieschang, J. Pflaum and M. Halik, *Nature*, 2007, **445**, 745-748.
55. I. McCulloch, M. Heeney, C. Bailey, K. Genevicius, I. MacDonald, M. Shkunov, D. Sparrowe, S. Tierney, R. Wagner, W. Zhang, M. L. Chabinyc, R. J. Kline, M. D. McGehee and M. F. Toney, *Nat. Mater.*, 2006, **5**, 328-333.
56. B. de Boer, A. Hadipour, M. M. Mandoc, T. van Woudenberg and P. W. Blom, *Adv. Mater.*, 2005, **17**, 621-625.
57. F. Mizutani, Y. Sato, S. Yabuki, T. Sawaguchi and S. Iijima, *Electrochim. Acta*, 1999, **44**, 3833-3838.
58. Z.-P. Li, Q.-H. Wu, C. Wang and Y.-Q. Su, *Anal. Sci.*, 2006, **22**, 763-767.
59. R. Barbucci, M. J. M. Campbell, M. Cannas and G. Marongiu, *Inorg. Chim. Acta*, 1980, **46**, 135-138.
60. J. C. M. J. N. Miller, *Statistics and Chemometrics for Analytical Chemistry*, Pearson/Prentice Hall, Upper Saddle River, N.J., 2005.
61. C. Li, S. Huang, C. Min, P. Du, Y. Xia, C. Yang and Q. Huang, *Polymers*, 2018, **10**, 24.
62. S.-i. Ishiguro, Y. Oka and H. Ohtaki, *Bull. Chem. Soc. Jpn.*, 1984, **57**, 391-394.